

# STRIP ANTENNA FIGURE ERRORS DUE TO SUPPORT TRUSS MEMBER LENGTH IMPERFECTIONS

Gyula Greschik\*,  
Martin M. Mikular\*\*, Richard G. Helms†, and Robert E. Freeland‡

## ABSTRACT

The dependence of strip antenna steady state geometric errors on member length uncertainties in the supporting truss beam is studied with the Monte Carlo analysis of a representative truss design. The results, presented in a format streamlined for practical use, can guide the specification for hardware fabrication of required error tolerances (for structural properties as well as member lengths), or they can aid the prediction of antenna performance if component statistics are available.

The standard rms error and locally defined errors are both considered. (The latter quantify surface and slope discontinuities between truss/antenna bays — discontinuities that may limit the effectiveness of some electronic error compensation schemes.) Second order global error compensation along the antenna length is also simulated.

The judicious definition of normalized variables leads to a straightforward set of scaling laws that easily relate the results to various truss dimensions and member length error magnitudes for trusses up to 100 bays long. The data pools on which quantitative observations are based are each populated by 35,000 (thirty-five thousand) to 3,465,000 (nearly three and a half million) elements.

## NOMENCLATURE

|  |   |
|--|---|
| $n, m$   | number of bays in the entire truss and in a segment (subtruss)  |
| $a$  | truss cross section edge (batten length)  |
| $L, l_{bay}, l$                                  | truss, bay, and subtruss lengths  |
| $N$  | number of subtrusses  |
| $e, \varepsilon_{rms}$                           | generic error symbol and rms surface error  |
| $\lambda, G$                                     | RF wavelength, antenna gain   |
| $\lambda_d, \lambda_e$                           | scaling coefficients for global dimensions and member length errors   |
| $f()$  | probability density function  |
| $\Delta l_{max}$                                 | maximum member length error magnitude   |
| $\underline{\mathbf{a}} = (a_i)$                 | vector of reference surface parameters $a_i$  |
| $\underline{\mathbf{b}}, \underline{\mathbf{A}}$ | vector and matrix quantities for rms surface error assessment   |
| $\alpha_{ij}, \beta_i$                           | elements of $\underline{\mathbf{A}}$ and $\underline{\mathbf{b}}$ , evaluated via integration over the antenna aperture |
| $\zeta$  | additional parameter for rms surface error assessment   |
| $s_{bay}, w_{bay}, w_{pan}$                      | bay sag, bay twist, and panel twist   |

---

\* Research Associate, University of Colorado.

\*\* Professor Emeritus, University of Colorado.

† Member Technical Staff, NASA JPL.

‡ Technical Manager, NASA JPL.

## INTRODUCTION

As is the case with all new structural applications, the engineering of long strip antennas, Fig. 1 (a), for space to meet emerging defense and scientific needs faces a number of unique challenges. Among these challenges are extreme aspect ratios and dimensions (lengths  $L > 80\text{ m}$ ). At the same time, the ever increasing pressure for cost and weight efficiency has prompted the consideration of space-rigidized technologies for critical structural members. However, space-rigidization has a limited track record in precision structures. Combining this emerging technology of yet uncertain geometric and structural reliability with (a) extreme geometries and (b) the need for application accuracy keenly raises the question of how component precision affects the accuracy of the whole. The present work offers quantitative insight into this statistical relationship via the Monte Carlo method for a selected configuration and error compensation, yet in a manner relevant to many mission conditions and designs. Wide practical scope is achieved by the careful definition of the antenna error measures and of the statistical characteristics of the error sources, which contribute to rendering the results scalable. Further, the simplicity of the truss configuration studied renders the results a convenient baseline of general interest.

### **Global through local antenna errors**

Two types of antenna errors are considered: the *rms* surface error and a few strictly local measures, the latter defined to assess (a) inaccuracies in the suspension of single antenna panels and (b) how well adjacent panels can be aligned. The *rms* error  $\varepsilon_{\text{rms}}$  is evaluated not only for the entire antenna, as commonly done, but also locally for antenna subsections. All subsections that can be possibly defined by truss bays within the entire antenna strip are statistically considered for a quasi-continuous view of the transition between local and global inaccuracies.

As the response of a truss beam section to strut errors is practically independent of the inaccuracies outside the section itself, error statistics for one section are equivalent to those for a complete, shorter, truss of the same length. Therefore, the Monte Carlo analysis of a single antenna design with error statistics processed for all its subsections is equivalent to studying all shorter antennas with the same bay architecture. Accordingly, the present study directly addresses one antenna design only, long enough to serve as a likely upper bound on all foreseeable practical designs. Namely, a length of 100 bays is considered. With the bay aspect ratio defined by equal longeron and batten lengths, this number corresponds to a truss length to diameter ratio  $L/D > 100$ , beyond the range typically considered practicable in a precision context.

### **Immaterial dimensions**

That antenna (truss) length in the previous section was referred to not with physical units (*meter*, *foot*, or similar) but with the number of bays was not accidental. Via a scaling principle (and associated scaling laws) presented below, it is made apparent that the error measures herein used, including  $\varepsilon_{\text{rms}}$ , depend on the number of truss bays, rather than physical length — provided that the strut errors are defined in absolute, as opposed to length proportional terms. This principle is well exploited in the present work by rendering absolute dimensions immaterial.

### **The Monte Carlo study**

The Monte Carlo study, where random effects are explicitly modeled with a multitude of analyses and then the results are statistically evaluated, has been chosen for the present investigation

for programming and engineering convenience and for adaptability to design modifications and later needs, including those of final design. The reference model, systematically perturbed with imperfections, is the simplest possible symmetric truss beam of triangular cross section with one diagonal per bay on the sides but, for symmetry, two on the base where the antenna is located. Cross section stiffness is identical in all members, and the battens are as long as the longerons.

The actual physical properties of the numerical model are immaterial in the context of the scaling laws used. Nevertheless, there are listed here for completeness:

- longeron and batten lengths  $l_{\text{longeron}} = l_{\text{batten}} = 1 \text{ m}$  — which made the entire truss length  $L=100 \text{ m}$  (for 100 truss bays)
- material Young's modulus  $E=210 \text{ GPa} \approx 30 \text{ million psi}$
- member cross section area  $A=6 \text{ mm}^2 \approx 0.0093 \text{ in}^2$

In the study, all member lengths were subjected to random errors of uniform distribution characterized by the same maximum magnitude along the truss. Pools of 35,000 (thirty-five thousand) truss models were analyzed for simulations of each of two electronic error correction schemes: !

- No error compensation. The *rms* surface error is simply evaluated with respect to a flat antenna reference surface.
- Quadratic error compensation, simulated by evaluating  $\epsilon_{\text{rms}}$  with respect to a reference surface parabolic in the truss axial direction.

Among other details, the results reveal that the *average* expectable  $\epsilon_{\text{rms}}$  error is below twenty times the  $\Delta l_{\text{max}}$  maximum length error magnitude for individual members even in the worst case scenario, when no error compensation is used and the truss is 100 bays long. In the same condition, the error associated with a 99.9% design certainty is still less than sixty times greater than  $\Delta l_{\text{max}}$ . These numbers greatly improve for shorter trusses (trusses of fewer bays) and as a result of quadratic error correction which generally reduces effective errors with more than 60%. However, the effectiveness of compensation gradually diminishes for shorter trusses, especially under 20 bays.

### ANTENNA ERRORS

The advancement of signal processing and electronic error correction techniques over the last few decades has much decreased the critical significance of certain imperfections of the structural geometry. Geometric errors, however, still remain of interest for two reasons. They continue to be a design concern, first, because the effectiveness of error compensation generally depends on error magnitudes, spatial frequency contents, distribution, and transient characteristics. Second, the sufficient control of geometric errors, if possible, can potentially eliminate altogether the need for electronic compensation in certain applications, thereby reducing system complexity and cost.

For the antennas herein considered, compensation is effective for error components of low spatial frequencies, cf. Fig. 1 (b) 2–3. On the other hand, high frequency components such as those dominating the illustrations in Fig. 1 (b), 4–6, cannot be corrected and are, therefore, of critical concern. In the present study where imperfections are accounted for via a general Monte Carlo analysis, low and high frequency error contributions are not artificially separated or filtered. Rather,

local and global errors, and the effectiveness of compensation are concurrently gauged with the application of two kinds of error measures: the “standard” rms surface error  $\varepsilon_{\text{rms}}$  in both global and local contexts, and a handful of carefully defined strictly local measures.

### **Rms surface error: definition and significance**

The “root-mean-square” recipe for error norms

$$\varepsilon_{\text{some}} = \sqrt{\frac{\int e_{\text{some}}^2 dA_{\text{some}}}{A_{\text{some}}}} \quad (1)$$

where  $e_{\text{some}}$  is some error measure (e.g., offset from the ideal surface in a given direction) and  $A_{\text{some}}$  is some measure of the antenna surface (e.g., the actual curved surface area of a dish) allows many possible error definitions. However, the only radiometrically meaningful option is <sup>1</sup>

$$\varepsilon_{\text{rms}} = \sqrt{\frac{\int (\Delta l / 2)^2 dA}{A}} \quad (2)$$

with  $\Delta l$  the optical path length change due to the errors and  $A$  the aperture. With the *rms surface error* according to Eq. 2, the loss of antenna gain  $G$  due to the imperfections is

$$G / G_0 = \exp(-[4\pi\varepsilon_{\text{rms}}/\lambda]^2) \quad (3)$$

where  $G_0$  and  $\lambda$  are the gain for the ideal geometry and the wavelength. (Note that Eq. 2 assumes uniform reception efficiency over the aperture. In the general context <sup>1</sup>, variable efficiency can be accounted for with a weighting-function coefficient to  $dA$ .)

In a realistic design context (where no “absolute” surface is explicitly given and the feed position can be adjusted for best performance) the parameters defining the reference surface from which the *rms error* is taken are determined by minimizing the *rms error* itself. If the surface is a plane — as is the case for a flat strip antenna — then three parameters must be set to minimize  $\varepsilon_{\text{rms}}$ . If, however, the reference surface is enriched with an extra parameter to render it parabolic in one direction (e.g., along the antenna length, to simulate second order error correction), then this extra geometric degree of freedom permits  $\varepsilon_{\text{rms}}$  to be lowered further.

Planar lens or phased array vs. reflector dish antennas. The derivation of Eqs. 2 and 3 is easily available for parabolic reflector antennas <sup>1</sup> where

$$\Delta l = 2 \Delta z \cos^2 \alpha \quad (4)$$

with  $\Delta z$  the offset from the ideal surface in the dish axial direction, and  $\alpha$  the paraboloid meridian slope angle (which disappears at the apex) <sup>2</sup>. However, efforts during this project succeeded neither to locate a derivation for strip lens and phased array antennas similar to Ruze’s <sup>1</sup>, nor to verify the validity of the fundamental gain expressions on which Ruze relies in the present context. Therefore, for the purpose of this work the gain expressions used by Ruze were simply assumed to apply, from which Eqs. 2 and 3 ultimately follow for strip antennas as well.

However, in the present context of a flat surface antenna, the optical path change simply equals the  $\Delta z$  offset in the normal direction of the actual antenna surface  $z(x, y)$  from the ideal  $z_0(x, y)$ :

$$\Delta l = \Delta z = z - z_0 \quad (5)$$

if the direction of transmission/sensing is perpendicular to the surface — the orientation that governs the errors for phased array operation. It is not surprising that the optical path change due to geometric errors for a surface antenna, Eq. 5, is nearly half that for a reflector, Eq. 4, because reflectors “fold the optical path” back over itself, and thus their surface aberrations cumulatively change *both* the incident and reflected segments of the path.

The *rms* error as defined by Eqs. 2 and 5 is illustrated in Fig. 2 (a) for a symmetric parabolic truss camber, with no twist or other additional deformation components. The  $\varepsilon_{\text{rms}}$  expressed as a function of the  $\delta$  bow,  $\varepsilon_{\text{rms}} = \delta/(3\sqrt{5})$ , depends only of the deformation magnitude  $\delta$  and is independent of structural dimensions.

In thin lens antennas, lens geometry errors effect wavefront errors roughly two orders of magnitude smaller than the surface imperfections themselves. Thus the dominating errors are not those of the lens but of the feed. In this case, Eqs. 2 and 5 apply to the feed surface. The context and details of the present work warrant that the results and observations presented below, while directly related to phased array operation, are also applicable to lens antennas.

The numerical assessment of the *rms* surface error. In realistic conditions the truss (slightly) bends and twists in all directions from bay to bay due to member length irregularities as indicated in Fig. 2 (b). The actual antenna surface, comprised of panels linked to one another and attached to truss joints, will depend on panel mechanics and suspension. For simplicity and generality, no details of this dependence are addressed here when the *rms* error is calculated. Instead, antenna panels are defined geometrically as bilinear rectangles stretched between the appropriate truss joints (intersections of truss member centerlines) in each truss bay, Fig. 2 (b). This definition is a good generic approximation. The effects of its differences from any particular design scenario quickly diminish with the increase of the number of panels considered.

In the frame of reference shown in Fig. 2 (b), where the axis  $x$  points along the antenna strip and the latter faces in the  $z$  direction, the reference (ideal antenna) surface — from which the errors are measured — is a plane

$$z_1(x, y) = a_0 + a_x x + a_y y \quad (6)$$

defined by the three coefficients  $a_0$ ,  $a_x$ , and  $a_y$ . These coefficients must be determined to minimize

$$\varepsilon_{\text{rms}} = \sqrt{\frac{\int (z(x, y) - z_1(x, y))^2 dA}{4 A}} = \frac{1}{2} \sqrt{\frac{M}{A}} \quad (7)$$

wherein  $z(x, y)$  is the actual imperfect antenna surface and

$$M = \int (z(x, y) - a_0 - a_x x - a_y y)^2 dA \quad (8)$$

With the expansion of the integrand this becomes

$$M = \zeta - 2 \underline{\mathbf{a}}^T * \underline{\mathbf{b}} + \underline{\mathbf{a}}^T * \underline{\mathbf{A}} * \underline{\mathbf{a}} \quad (9)$$

where the asterisk and superscript  $T$  denote the inner (dot) product and the matrix transpose, and the vector and matrix variables  $\underline{\mathbf{a}}$ ,  $\underline{\mathbf{b}}$ , and  $\underline{\mathbf{A}}$  are

$$\underline{\mathbf{a}} = \left( a_0 \quad a_x \quad a_y \right)^T \quad (10)$$

$$\underline{\mathbf{b}} = \left( \beta_0 \quad \beta_x \quad \beta_y \right)^T \quad (11)$$

$$\underline{\underline{\mathbf{A}}} = \begin{bmatrix} \alpha_0 & \alpha_x & \alpha_y \\ \alpha_x & \alpha_{xx} & \alpha_{xy} \\ \alpha_y & \alpha_{xy} & \alpha_{yy} \end{bmatrix} \quad (12)$$

with

$$\left. \begin{aligned} \alpha_0 &= \int 1 dA &= \mathbf{A} \\ \alpha_x &= \int x dA \\ \alpha_y &= \int y dA \\ \alpha_{xx} &= \int x^2 dA \\ \alpha_{xy} &= \int x y dA \\ \alpha_{yy} &= \int y^2 dA \end{aligned} \right\} \quad (13)$$

$$\left. \begin{aligned} \beta_0 &= \int z dA \\ \beta_x &= \int x z dA \\ \beta_y &= \int y z dA \end{aligned} \right\} \quad (14)$$

$$\zeta = \int z^2 dA \quad (15)$$

Minimizing  $\varepsilon_{\text{rms}}$  is equivalent to minimizing  $M$ . Accordingly requiring that the partial derivatives  $\partial M/\partial a_0$ ,  $\partial M/\partial a_x$ , and  $\partial M/\partial a_y$  of Eq. 9 disappear, one obtains

$$\underline{\underline{\mathbf{A}}} * \underline{\mathbf{a}} = \underline{\mathbf{b}} \quad (16)$$

Once the coefficient matrix, the right hand side, and  $\zeta$  are known (Eqs. 13 through and 15), the parameters  $a_0$ ,  $a_x$ , and  $a_y$  to determine the reference plane are given by Eq. 16 in the context of the  $(x, y, z)$  coordinate system used. The *rms* surface error consequently follows from Eqs. 7 and 9.

Pivotal to this procedure is the calculation of the integrals Eqs. 13 through 15 which must be performed numerically. In the present work, this was accomplished with two-point Gauss quadrature in two dimensions over each antenna panel as defined in Fig. 2 (b). This meant four integration points per truss bay. The accuracy of this procedure proved excellent. A comparison with the mid-point rule revealed that  $40 \times 40 = 1600$  integration points *per each panel* were required in the latter to reduce the errors between the two approaches to below 0.1%.

Integration was performed over the perfect, undeformed, aperture  $A = L a$  (cf. Fig. 1 (a)). In-plane surface error components (in the  $x$  and  $y$  directions) were ignored as higher order effects.

Error compensation. The procedure described in the previous section addresses “absolute” surface errors, with respect to an ideally flat antenna reference surface. However, electronic error compensation can effectively remove some low spatial frequency components from the error pattern. This reduction of the error space can be simulated by using a reference surface with geometric degrees of freedom appropriately increased from the three ( $a_0$ ,  $a_x$ , and  $a_y$ ) associated with the flat geometry and then minimizing  $\varepsilon_{\text{rms}}$  with this extended set of parameters.

A first level error correction is quadratic compensation along the antenna strip (“linear correction” is trivially performed by antenna orientation and is inherently accounted for in the previous section). For the simulation of this correction mode, the reference surface is extended with a quadratic

term in  $x$

$$z_2(x, y) = a_0 + a_x x + a_{xx} x^2 + a_y y \quad (17)$$

which increases the number of surface parameters to four:  $a_0$ ,  $a_x$ ,  $a_{xx}$ , and  $a_y$ , cf. Fig. 2 (b). The calculation proceeds as for the planar reference surface except for changes stemming from the replacement of  $z_1(x, y)$  in Eq. 7 with  $z_2(x, y)$  of Eq. 17. Thus  $M$  becomes

$$M = \int (z(x, y) - a_0 - a_x x - a_{xx} x^2 - a_y y)^2 dA \quad (18)$$

The form of Eq. 9 does not change, but the involved quantities now become

$$\underline{\mathbf{a}} = \begin{pmatrix} a_0 & a_x & a_{xx} & a_y \end{pmatrix}^T \quad (19)$$

$$\underline{\mathbf{b}} = \begin{pmatrix} \beta_0 & \beta_x & \beta_{xx} & \beta_y \end{pmatrix}^T \quad (20)$$

$$\underline{\underline{\mathbf{A}}} = \begin{bmatrix} \alpha_0 & \alpha_x & \alpha_{xx} & \alpha_y \\ \alpha_x & \alpha_{xx} & \alpha_{xxx} & \alpha_{xy} \\ \alpha_{xx} & \alpha_{xxx} & \alpha_{xxxx} & \alpha_{xxy} \\ \alpha_y & \alpha_{xy} & \alpha_{xxy} & \alpha_{yy} \end{bmatrix} \quad (21)$$

which include the following parameters not yet defined earlier:

$$\left. \begin{aligned} \alpha_{xxx} &= \int x^3 dA \\ \alpha_{xxxx} &= \int x^4 dA \\ \alpha_{xxy} &= \int x^2 y dA \end{aligned} \right\} \quad (22)$$

$$\beta_{xx} = \int x^2 z dA \quad (23)$$

The numerical integration of these quantities is as for those in Eqs. 13 through 15, and the reference surface parameters Eq. 19 are solved from Eq. 16, naturally interpreted in the present quadratic (4-dimensional) context.

Local vs. global errors. As alluded to above, high spatial frequency (local) shape inaccuracies are of special concern. One way of illuminating local error magnitude is via calculating as described above the *rms* surface error  $\varepsilon_{\text{rms}}$  for limited antenna sections.

Generally, several sections defined by a certain length (a certain number of bays) can be associated with any particular truss. As illustrated in Fig. 3 (a), a section (subtruss) can be considered to start at the truss end, or after the first bay, and so forth. For a truss  $n$  bays long there are exactly

$$N_m = n - m + 1 \quad (24)$$

different (but overlapping) subtrusses of  $m$  bays each. (If subtruss length may vary from one bay through the entire truss length — in the last case the entire truss is the “subtruss” — then the total number of all possible subtrusses is

$$N_{\text{all}} = \sum_{m=1}^n N_m = n(n+1)/2 \quad (25)$$

which grows quadratically with the total number of bays  $n$ .)

In the error analysis below, the entire spectrum of local through global errors will be surveyed by evaluating  $\varepsilon_{\text{rms}}$  for every one of the  $N_{\text{all}}$  possible subtrusses along each antenna model considered. For each of these calculations, the substructure deformations will be treated independently, stripped of the global structural context. The various subtrusses so defined (overlapping within each global truss analyzed) will then be placed into data pools according to subtruss length, to be processed as undistinguished statistical entities within each pool.

The treatment just outlined ignores that, actually, not all subtrusses are independent. One form of interdependence is due to substructure overlap (more precisely, to the overlap of substructure deformation fields) within each global truss solution. Another, very subtle, flaw in the data pool is a possible lack of mechanical uniformity between subtrusses within a redundant truss as follows.

If the truss is statically indeterminate then the effects on local truss deformations of a particular strut length error depend on the location along the truss beam: local deformations are somewhat better constrained by the adjacent bays near the center than near the end, Fig. 3 (b). Therefore, the response in a subtruss near the antenna end to a certain kinematic load pattern differs from a similar one near midspan. This non-uniformity of the subtruss statistical data pools is acknowledged with concurrently emphasizing that its effects are generally insignificant.

Possible non-uniformities in the statistical pools and interdependence between some of their elements, however, are not a concern for the present study because we do not seek a precise mapping of truss geometric errors but a generic assessment of inaccuracies over antenna segments of various lengths. On the level of generality pursued, there is no justification to distinguish between or to weight locations along the truss. Therefore, the way the statistical data pools are constructed is appropriate, and the concept of subtruss sets of various lengths is sufficiently refined to quantitatively illuminate the relationship between local and global *rms* errors.

### **Some strictly local error measures**

As outlined above, the need for information on local imperfections is herein addressed with the *rms* surface error by evaluating  $\varepsilon_{\text{rms}}$  both locally and globally. However, while generating the  $\varepsilon_{\text{rms}}$  norm, the definition Eq. 2 also works as a “mathematical filter” by concealing the details of the error pattern. Some of the lost information — such as individual panel deformations and the differences of orientation between adjacent panels — may be potentially critical for structural as well as electronic system design.

Three strictly local error measures are hereby defined to statistically capture such details. As the purpose of these measures is not to directly support any specified design or analysis procedure but to capture otherwise lost technical information, their definition is not streamlined for any particular use or algorithm. Rather, they are crafted solely to capture *all aspects* of local (bay-to-bay) deformations that may be potentially relevant for yet unspecified future use. The normalization (non-dimensionalization) of these measures serves the convenience of definition, as opposed to that of an governing algorithm. These measures provide all information possibly necessary for quantifying local out-of-plane errors such as

- The deformations of flexible panels firmly held at all corners.
- Out-of-plane edge and corner offsets between adjacent rigid panels with all possible patterns of

three-point suspension.

- Orientation errors between adjacent panels.
- Other similar imperfections.

The errors (their statistical characteristics) presented below should be transformed (scaled and/or combined) to meet design needs once the latter is defined.

These three local errors are introduced in Fig. 4 in the direct physical context, without normalization. The first two, the *bay sag* and the *bay twist*, Fig. 4 (a) and (b), capture the orientation errors between pairs of adjacent panels in the axial and lateral directions, respectively. As indicated in the figure, both are defined via how (axial or lateral) centerlines in adjacent panels are oriented with respect to one another. (This definition reflects the features of the assumed bilinear panel geometry, cf. Fig. 2 (b).)

Bay sag relates the two panel orientations with the offset  $s_{\text{bay}}$  in the  $z$  direction of the shared endpoint of the axial centerlines from the line subtended by their other endpoints. The bay twist  $w_{\text{bay}}$ , in turn, quantifies the relative error of the lateral orientations via the out-of-flatness of the rectangle subtended by the two lateral centerlines. This out-of-flatness, defined as shown in Fig. 4 (b), reveals how much steeper one panel is than the other in the lateral direction.

Note that both orientation errors are quantified via length, as opposed to angular, quantities. This is critical for the convenience of scaling: as to be seen below, errors so defined turn out to not depend on truss bay dimensions if some simple guidelines are followed. Despite their definition via length quantities, however, these measures are mathematically equivalent to any angular measure one may prefer in the sense that any angular orientation error between the panels can be calculated from  $s_{\text{bay}}$  and  $w_{\text{bay}}$  (in the context of the truss geometry).

The third error, the panel twist  $w_{\text{pan}}$ , captures panel out-of-flatness via how much one panel corner is off in the  $z$  direction from the plane subtended by the other three, Fig. 4 (c). This error shows how much a flexible antenna panel, firmly attached to truss joints at all corners, would twist — or, equivalently, what the corner offset (surface “step”) between adjacent rigid panel surfaces would be if the latter were attached to the truss via three-point suspension. While the sign of  $w_{\text{pan}}$  does, its magnitude does not depend on which of the four corners is considered.

### MONTE CARLO STUDY

To illuminate the statistical characteristics of the above error measures, a Monte Carlo study designed for the general applicability and the scalability of the results has been performed.

An alternative would have been a probabilistic study either on purely theoretical grounds, or with some numerical assistance. Theoretical routes <sup>3</sup>, dominant before low-cost electronic computing, are limited by the assumptions they invoke to enable the problem’s solution. Numerical work in direct support of probability theory, also characteristic to early statistical engineering <sup>4</sup>, still requires careful mathematical manipulation for each statistical result (error measure) examined. Moreover, both of these options limit the statistical model of the error sources, permitting the change of their probabilistic distributions and key parameters only at the cost of an overhaul of the entire procedure. Its computational and mathematical robustness, algorithmic simplicity, and universal applicability to all probabilistic conditions and contexts rendered the Monte Carlo method ideal

for the present work.

### Modeling assumptions

For the general applicability and scalability of results, the truss design and member length error distributions modeled are the simplest possible. The design, shown in Fig. 5 (a), is characterized by equal longeron and batten lengths, equal member cross section stiffnesses in all members, and left-right symmetry. (A corollary of this symmetry is the redundancy of diagonals on the lower face, where the antenna is located.)

Member length irregularities in real hardware would be associated with a number of systematic and random error sources including

- imperfect member length control during fabrication,
- joint inaccuracies,
- cross section imperfections and strut out-of-straightness,
- material non-uniformities (e.g., variations in the thermal expansion coefficient),
- and random aspects of deployment and space rigidization —

some of which influence member length only under certain environmental conditions — the latter not fully deterministic either. The combined impact of these influences on member length is likely to result in distribution similar to the normal (Gaussian) curve, shown without systematic error by the first inset in Fig. 5 (b). Actually, as outstanding errors are eliminated by quality control during fabrication, the model shown in the second inset in the same figure — standard distribution with the extreme values eliminated — would be more realistic.

For simplicity and conservativeness, however, the distribution is modeled as symmetric and uniform, cf. Fig. 5 (b). (Note that, if fabrication quality control is sufficiently stringent with respect to the error scatter controlled, then this approximation becomes increasingly realistic and its conservative edge diminishes.)

The irregularities are modeled as length, as opposed to strain errors — which renders them absolute, rather than length-proportional. Such errors are typically due to joint and assembly imperfections, while length-proportionality is characteristic of most other error sources. For the modeled truss configuration, however, where all longerons and battens are of the same length, the difference between the two options is not dramatic. Absolute errors are preferred in the present work because of the scaling convenience they offer — namely, they render the *rms* surface error and the other, local, error measures *independent of the bay/strut dimensions*, as discussed below.

### Scaling principle

The conditions of (a) uniform cross section stiffnesses, (b) one given truss architecture with a constrained bay aspect ratio ( $l_{\text{bay}} = a$ ), and (c) an identically uniform and symmetric absolute length error distribution for all members, concurrently enable a convenient scaling of structural responses, including error statistics. To introduce the principles of this procedure, we begin with relating two trusses with certain rules of proportionality between, and then apply the results to statistical analysis.

Within the framework of the above conditions for structural configuration and error definition, take two trusses of the same number of bays and refer to one as the “reference,” the other as the

“companion” truss. Let the proportionality between the two geometries, guaranteed by the equality of bay numbers, be defined with the coefficient  $\lambda_d$  as indicated in Fig. 6 so that a generic dimension  $d$  in the reference design scales with  $\lambda_d^{-1}$  to the corresponding companion dimension  $d_s$ :

$$d_s = \lambda_d^{-1} d \quad (26)$$

Further, subject the two trusses to sets of kinematic loads (member length errors) proportional with coefficient  $\lambda_e^{-1}$  such that for corresponding length errors  $e$  and  $e_s$

$$e_s = \lambda_e^{-1} e \quad (27)$$

as illustrated in Fig. 6. Note that, according to scaling conventions, a  $\lambda_i > 1$  scaling coefficient corresponds to scaling *down* to magnitudes smaller than the original.

A scrutiny of various possible truss responses similar to what led to the formulation of the constant thickness scaling laws<sup>5,6</sup> reveals scaling laws between the two trusses, some of which are listed in Table 1 without detailing their derivation. To better illuminate the contents of the table, consider that

- The “immaterial” nature of cross section stiffnesses means that these can be set independently and arbitrarily in the two trusses, without affecting the scaling laws (the rest of the table).
- Stresses are “underdetermined” in that they are not fully defined by the available information. They also depend on cross section stiffness.
- Various parameters of length units — displacements, the *rms* error, and the local antenna errors defined above — do not depend on  $\lambda_d$ . This independence from how the overall geometry is scaled is a remarkable corollary of defining strut length imperfections as absolute, as opposed to length-proportional (strain) errors.

The significance of these scaling laws for individual responses to statistical analysis is straightforward. Namely, as the results of each analysis in a Monte Carlo study (for an appropriately designed truss) can be scaled to any given similar truss with different dimensions and error length magnitudes, the statistical parameters scale accordingly (because all standard statistical parameters scale with the data pool).

In other words, each statistical result scales according to the law in Table 1 spelled out for the response to which it relates. Further, as in the present work each error measure of statistical interest has been defined with length units, the associated statistics depend on the strut length errors only, and *are independent of the truss size*.

### Software toolkit

All analyses and statistical processing for the present project have been performed with software newly written for this very specific purpose. The integrated package included a linear FEA program, a truss pre-processor module, and a statistical analysis driver. All program units were written in the C language and run on Linux. This approach ensured very high computational efficiency, necessary for the massive amounts of data produced, as well as direct control over computational accuracy and statistical details. Graphical postprocessing (the visualization of the results, including generating the images of deformed trusses) was assisted by Perl scripts and relied on the *gnuplot* plotting utility.

The software was designed, written, and tested with a somewhat modular approach to facilitate its future application to models and problems different from the present. Therefore, it can be modified with relative ease to model statistical error sources and/or truss architectures and properties other than those examined here. One possible future application is the support of the final/detailed design of specific long strip antenna support trusses.

## ANALYSIS, RESULTS, AND DISCUSSION

In most cases, a few hundred analyses are sufficient in a Monte Carlo study to assess mean values<sup>7</sup> — of errors or other parameters alike. The present study, however, aims not at simply gauging the direct average of selected responses, but also to guide future design with reliable data and to give confidence to the specification of component tolerances in light of global error requirements and failure probabilities. This requires a rich statistical pool, set for the present work to a total of 35,000 (thirty-five thousand) randomly perturbed truss models for the simulation of each of the considered two electronic antenna error correction schemes:

- No error compensation. The *rms* surface error is simply evaluated with respect to a flat antenna reference surface.
- Quadratic error compensation, simulated by evaluating  $\epsilon_{\text{rms}}$  with respect to a reference surface parabolic in the truss axial direction.

However, as it will be seen, even this data pool should be improved to better support some of the observations made.

(Actually, the size of the analysis pool was set to 35,000 not by probabilistic considerations but simply by software and hardware limitations. Within the framework of the data management and computational approach adopted, the computer hardware and operating system permitted no further increase of the data set. Methods to overcome this limitation should be explored if further or more detailed information will be required.)

The models' physical properties, immaterial in the context of the scaling laws outlined above, were

- longeron and batten lengths  $l_{\text{long}} = l_{\text{bat}} = 1 \text{ m}$  (making the truss length  $L=100 \text{ m}$ , for 100 bays),
- material Young's modulus  $E=210 \text{ GPa} \approx 30 \text{ million psi}$ , and
- member cross section areas  $A=6 \text{ mm}^2 \approx 0.0093 \text{ in}^2$ .

The maximum magnitude of length errors, limiting the random length errors in the positive and negative directions, was  $\Delta l_{\text{max}} = 10^{-4} \text{ m} = 0.1 \text{ mm} \approx 4 \text{ mils}$  in all struts. While this error corresponds to  $\epsilon = 10^{-4}$  and  $\epsilon = 0.707 \times 10^{-4}$  strains in the longerons/battens and in the diagonals, respectively — values conservatively realistic for space thermal conditions — the value of  $\Delta l_{\text{max}}$  will be rendered immaterial by using it as the basis of normalization for all responses of interest (cf. the scaling laws described above).

### **Illustration via truss examples**

The first twelve of the 35,000 truss models generated by random strut length errors (as discussed above) are shown in Fig. 7 via a side view with the deformations increased hundred-fold. Also depicted is for each model the ideal (reference) antenna surface from which the surface errors

are measured for the *rms* error (right side). The trusses are oriented for the surfaces to appear horizontal. However, the linear surface appearance is simply due to the lack of graphic detail — in reality, the surfaces are generally also (slightly) tilted laterally to minimize  $\varepsilon_{\text{rms}}$ .

The geometric simulation of quadratic error correction for the trusses of Fig. 7 is illustrated in Figs. 8 where the reference surfaces are parabolic in  $x$ . The added curvature enables these surface to much better approach the crooked truss shapes and thereby much better lower antenna surface offsets and  $\varepsilon_{\text{rms}}$  to the values shown on the right. (As these surfaces are nearer to the truss shapes as the flat references in Fig. 7, their visibility is enhanced by indicating the truss shape with the battens only, without diagonals and longerons.) The parabolic reference surface accomplishes geometrically exactly what second order electronic error correction does via signal processing: the removal of the parabolic terms from the global error pattern. The higher order errors to remain after this removal are the antenna's offset from the parabolic reference, shown in Fig. 9 via the distortion of the truss and reference shapes of Fig. 8 to render the latter appear flat. This effective residual error is dramatically lower than the uncorrected out-of-flatness, Fig. 7.

### ***Rms* error probabilities**

As discussed above, *rms* surface errors have been assessed for each of the 35,000 truss models for all possible subtrusses up to the entire truss length, and subtrusses of identical lengths were placed in data sets to be treated independent of one another. By revealing  $\varepsilon_{\text{rms}}$  distributions for various numbers of truss bays, this approach provides insight into how local and global errors relate in a long truss — or, equivalently, how truss length influences accuracy.

This relationship is shown via failure probability plots in Fig. 10. In particular, plotted are for each truss length the (normalized) error values that divide the data pools into specific fractions, indicated by the percentage values associated with each plot. For example, the threshold errors plotted as the “99.9%” curve separate the lower 99.9% of the specimen pool (with lower *rms* surface errors) from the top tenth of a percent (with greater errors). Such plots effectively show what error values correspond to certain likelihoods of success. The plots in Fig. 10 thus reveal what error limits are 95, 99, and 99.9% likely to be achieved by trusses of various lengths, and how accurate the average trusses will be.

Apparently, the *average* expectable  $\varepsilon_{\text{rms}}$  error is always below twenty times the  $\Delta l_{\text{max}}$  maximum length perturbation magnitude for individual members, and even the  $\varepsilon_{\text{rms}}$  associated with a 99.9% compliance certainty is less than sixty times the  $\Delta l_{\text{max}}$ . As expected, the worst case scenario is the longest truss (100 bays) with no error compensation. Performance greatly improves for shorter trusses (equivalently, shorter truss segments). The benefits of error correction can be seen by comparing the uncorrected results, Fig. 10 (a), with the corrected ones, Fig. 10 (b). Quadratic correction generally reduces effective errors with more than 60%. However, the effectiveness of compensation gradually diminishes for shorter trusses, especially under 20 bays.

Note that there is an “elbow region” in the plots both in the uncorrected and the corrected cases, roughly between 3–7 and 8–11 numbers of bays, respectively. The steeper plot regions to the right from these elbows are dominated by the primarily “bending” effects of the longeron length imperfections, while the “shear” effects by the errors in the other members dominate the left.

Recall that each possible subtruss, overlapping or not, is extracted for statistical processing from the global trusses analyzed. Consequently, the number of subtrusses increases with the decrease of

the subtruss length: the statistical data pool is increasingly richer toward the left sides in Figs. 10 (a) and (b). On the right ends, where the only “subtruss” is the entire truss itself, the data population is 35,000. The 99.9% probability curves thereat separate the top 35 specimens from this pool — a significant, albeit perhaps statistically still weak population. However, on the other extreme (truss lengths of 2 bays) the data population is 3,465,000, a nearly hundred-fold increase. The difference in statistical quality between the two ends of the spectrum is apparent on some details of the probability density functions for  $\varepsilon_{\text{rms}}$  discussed next.

### ***Rms* error probability densities**

How the surface errors are distributed within each subtruss data set is revealed by the standard probability density functions, shown for trusses 100, 70, 40, and 10 bays long in Figs. 11 and 12. These plots reveal the proportional likelihood of a random truss to have an error in the vicinity of the abscissa values, and were herein generated numerically by subdividing the sorted data sets into like-sized groups and then assessing the surface error average in each group. This somewhat non-standard approach to the calculation is computationally convenient but provides data resolution locally proportional to the value of the density plot. The associated “jitter” in the plots in Figs. 11 and 12 near their maxima is a result of this locally high data resolution. The statistical quality of the data populations (the numbers of specimens) is well revealed by the intensity of this local irregularity: the more populous data sets for shorter trusses are clearly smoother near their maxima than the others. (This trend may not be apparent on the plots from the least populous 100-bay long truss set because here the phenomenon is reduced with numerical damping, so disturbing was the irregularity without special measures.)

The probability density plots can be seen as “vertical” slices parallel to the ordinate axis across the failure probability plots in Fig. 10. Accordingly, the plot values given there can be identified on the probability density curves and are done so in Figs. 11 and 12 by small flag-like symbols indicating the average, as well as the 95, 99, and 99.9% threshold errors with linen codes similar to those used in Fig. 10.

### **The local errors**

The evaluations of the bay sag, bay twist, and panel twist are statistically and computationally simple in comparison to the *Rms* error because these measures have been defined strictly in the local context, see above. Their probability density plots, Fig. 13, are nearly Gaussian with no systematic error (with a zero mean). Their statistical characterization, therefore, can be easily summarized as in Table 2 and requires no explanation.

As alluded to above, the numbers in Table 2 along with the mathematics of the Gaussian distribution enable the derivation of any possibly relevant panel deformation or alignment error. The actual derivation will depend on the parameters of interest and it may require some considerations of probability theory and basic geometric transformations. However, no statistical evaluation will have to be repeated or redone for this work.

## APPLICATION EXAMPLES

The non-dimensional presentation and the straightforward scaling laws render the application of the Monte Carlo results simple, as illustrated below via three examples.

### Assessing figure error from member length imperfections — truss of 80 bays

Consider a truss of

- An architecture compatible with the assumptions of the present work (square bay aspect ratios  $l_{\text{bay}} = a$ , a topology as shown in Fig. 5 (a), and uniform member cross section stiffnesses.
- A total length of  $L=300$  m.
- Eighty bays  $n=80$ .

Therefore, the bay length and, consequently, the truss cross section sides, are

$$l_{\text{bay}} = a = L/n = 3.75 \text{ m} \quad (28)$$

Let the truss be subjected to uniformly random member length imperfections  $\Delta l$  which, for all members, are limited according to

$$-\Delta l_{\text{max}} < \Delta l < \Delta l_{\text{max}} = 0.5 \text{ mm} \quad (29)$$

Such errors may arise from a combination of fabrication imperfections, nonuniform mechanical (thermal) properties, assembly (joint) errors, and environmental effects (e.g., shading).

According to Fig. 10 (a), the normalized error thresholds ( $\varepsilon_{\text{rms}}/\Delta l_{\text{max}}$ ) achievable by an 80 bays long truss are approximately 12, 33, and 42 for average, 99%, and 99.9% certainty. Therefore, an antenna attached to the example truss would most likely have a  $\varepsilon_{\text{rms,avg}}=12 \times 0.5=6.0$  mm overall surface error, but it will achieve  $\varepsilon_{\text{rms,99\%}}=33 \times 0.5=16.5$  mm accuracy with 99% likelihood, and  $\varepsilon_{\text{rms,99.9\%}}=42 \times 0.5=21.0$  mm accuracy with 99.9% likelihood.

Quadratic error compensation will improve these numbers to  $\varepsilon_{\text{rms,avg}}=5.1 \times 0.5=2.5$  mm,  $\varepsilon_{\text{rms,99\%}}=12 \times 0.5=6.0$  mm, and  $\varepsilon_{\text{rms,99.9\%}}=16 \times 0.5=8.0$  mm, based on Fig. 10 (b). While this performance may be acceptable for an L-band radar application, it should be further improved with additional active (geometric or electronic) correction to satisfy X-band requirements. An immediate question is how far cubic correction — the next step beyond the herein discussed quadratic control — would go towards meeting X-band needs. This question, beyond the scope of the present work, is yet to be answered.

Note that the above example calculations concern figure errors over the entire antenna surface (length). Antenna *subsection* surface accuracy would be obtained from the same plots, sampled at the locations corresponding to the truss subsection length (number of bays).

### Assessing figure error from member length imperfections — truss of 40 bays

Consider a truss of the same architecture (bay topology and aspect ratios), same total length  $L=300$  m, and same absolute member length errors  $\Delta l_{\text{max}} = 0.5$  mm as in the previous example, but consisting of forty, as opposed to eighty, bays:  $n=40$ .

The bay length and the truss cross section sides thus are

$$l_{\text{bay}} = a = L/n = 7.50 \text{ m} \quad (30)$$

Note that, in comparison to the previous example, these struts are twice as long yet have the same absolute length errors. Member length accuracy for this truss is, therefore, relatively better controlled than for the 80-bays example.

To assess the uncorrected global errors, take Fig. 10 (a). From the plots one obtains that the normalized error thresholds ( $\varepsilon_{\text{rms}}/\Delta l_{\text{max}}$ ) achievable by a sequence of 40 bays are approximately 4.3, 12, and 15 for average, 99%, and 99.9% certainty. Consequently, an antenna attached to this example truss would most likely have a  $\varepsilon_{\text{rms,avg}}=4.3 \times 0.5=2.2 \text{ mm}$  overall surface error, but it will achieve  $\varepsilon_{\text{rms,99\%}}=12 \times 0.5=6.0 \text{ mm}$  accuracy with 99% likelihood, and  $\varepsilon_{\text{rms,99.9\%}}=15 \times 0.5=7.5 \text{ mm}$  accuracy with 99.9% likelihood. Quadratic error compensation will improve these numbers to  $\varepsilon_{\text{rms,avg}}=2 \times 0.5=1.0 \text{ mm}$ ,  $\varepsilon_{\text{rms,99\%}}=4.3 \times 0.5=2.2 \text{ mm}$ , and  $\varepsilon_{\text{rms,99.9\%}}=5.6 \times 0.5=2.8 \text{ mm}$ , based on Fig. 10 (b).

This performance is dramatically closer to X-band requirements than the 80-bays example. Note, however, that the observed improvement cannot be linearly related to the number of bays or the bay/strut dimensions. Performance is nonlinearly governed by these parameters.

### Design for specified wavelength and accuracy

Consider an example application at an RF frequency of  $f=12 \text{ GHz}$ , with a permissible *rms* figure error of one fifteenth the associated wavelength:

$$\varepsilon_{\text{rms}} = \lambda/15 \approx 2 \text{ mm} \quad (31)$$

Further, for the truss compatible with our current structural assumptions (square bays  $l_{\text{bay}} = a$ , topology as in Fig. 5 (a), and uniform cross section stiffnesses) assume that fabrication technology and environmental conditions limit the absolute strut length errors  $\Delta l$  to

$$-\Delta l_{\text{max}} < \Delta l < \Delta l_{\text{max}} = 0.5 \text{ mm} \quad (32)$$

regardless of strut length. The design to most economically serve the accuracy requirement is sought.

The member length and accuracy specifications Eqs. 31 and 32 define the normalized accuracy as

$$\varepsilon_{\text{rms}}/\Delta l_{\text{max}} = 4 \quad (33)$$

which, in turn, determines a distinct coordinate value on the normalized precision likelihood plots in Fig. 10. The associated horizontal lines, marked in Fig. 14 (a) and (b) for the uncorrected and corrected cases, are the graphical representation of the accuracy specification considered. The intersection points between these horizontal lines and the likelihood curves then exactly define how many truss bays are needed to achieve the desired accuracy with particular certainties. If no error compensation is used, then the number of truss bays must be no more than 15 for the desired  $\varepsilon_{\text{rms}} = \lambda/15 \approx 2 \text{ mm}$  accuracy to be achieved with a 99.9% or greater certainty — the normalized accuracy line intersects the 99.9% certainty curve at  $n \approx 15$  in Fig. 14 (a). Similarly, Fig. 14 (b) reveals that the number of truss bays can be increased to about  $n \approx 32$  for the same error certainty if quadratic compensation is used. (For a given length for the entire truss, increasing the number of bays means reciprocally decreasing the truss depth because the bay aspect ratio is constrained. This reciprocal scaling does not affect the total member lengths.)

Finally, the design condition illustrated in Fig. 14 is also shown in Fig. 15 in an alternative manner, where the surface error  $\varepsilon_{\text{rms}}$  is not normalized with the maximum member length error. The non-normalized certainty curves in this figure are applicable *only to the present example problem*

where  $\Delta l_{\max} = 0.5 \text{ mm}$ , as opposed to the normalized plots in the preceding figures which are generally applicable to all member length error magnitudes.

### CONCLUDING REMARKS

A simple graphical procedure has been established to guide the specification of truss member error tolerances or, alternatively, to aid the prediction of performance uncertainties for long antenna strips. This procedure is based on the results of a Monte Carlo analysis of 35,000 truss models, performed with dedicated FEA and statistical software. The applicability of the results, including the design plots, to various truss dimensions, strut length error magnitudes, and to trusses with different numbers of bays, is ensured by a non-dimensionalized approach and a set of carefully crafted scaling laws. These scaling laws are actually two sets of laws merged as they address the scaling of the structural dimensions and that of the member length errors concurrently, yet mathematically independent of one another. One striking consequence of these laws and of the choice of parameter definitions on which they are based is the revelation that global antenna surface errors (such as the *rms* error  $\varepsilon_{\text{rms}}$ ) *depend only on the number of truss bays, and not on the truss dimensions*, provided that the individual strut length errors are otherwise not changed.

The quantitative analysis has revealed that the *average* expectable  $\varepsilon_{\text{rms}}$  error is below twenty times the  $\Delta l_{\max}$  maximum strut length error magnitude even in the worst considered case when the truss is 100 bays long and the figure errors are not electronically compensated. In the same conditions, the error limit associated with 99.9% design certainty is still less than sixty times  $\Delta l_{\max}$ . These numbers greatly improve for trusses of fewer bays and as a result of quadratic error correction which generally reduces effective errors with more than 60%.

The quadratic error correction has been numerically modeled by removing polynomial terms up to the second order of the deformed truss shape along the truss length.

The results of the study have been summarized via certainty plots which reveal figure error probabilities as well as their dependence on strut error magnitudes, the number of truss bays, and error compensation. These plots are universally applicable to all truss dimensions, member stiffnesses, and most error sources (fabrication, thermal, or other) and are a straightforward tool for both preliminary design and error assessment. The report has concluded by illustrating the application of these plots to two engineering examples: one, where the likely errors and the effect of error compensation of a certain design were sought, the other, where the architecture to best satisfy a specified error tolerance was to be identified.

It would be highly desirable to complement these compelling results with:

- **Further error compensation schemes.**

Only one, the quadratic, error compensation scheme has been modeled. As a minimum, the effects of third order (cubic) compensation should also be assessed.

- **Theoretical analysis.**

Various characteristics of the statistical results are likely to be explainable with theoretical considerations, possibly providing practically significant insight beyond what has already been presented. Theoretical work should complement the Monte Carlo study.

- **Alternative length error distributions.**

The effects of systematic errors and member length perturbations statistically more complex than the uniform distribution should be addressed. At the minimum, the truncated normal distribution, the best approximation available for generic fabrication and environmental error sources, should be included in the study.

- **Alternative bay aspect ratios.**

Preliminary considerations have shown that simple design relations similar to the scaling laws herein presented may be derivable to support the extrapolation of the results to truss beams of different bay aspect ratios (where the longeron and batten lengths are not equal). This issue deserves careful attention because it may greatly increase the scope of the design procedure to more general truss geometries, and it may do so without greatly complicating the procedure already derived.

- **Data pools sufficiently large for all analytical needs.**

While the number of trusses (35,000) investigated has been sufficient in the contexts of most statistical needs, there are some exceptions with acute significance for the present design problem. In particular, the assessment of high probability certainties ( $\geq 99.9\%$ ) would clearly require more data. The computational and database limitations that forbade the present study to use greater data pools should be overcome.

#### ACKNOWLEDGMENTS

The research described in this paper was carried out by the Jet Propulsion Laboratory, California Institute of Technology, and its collaborators, under contract number \*\*\*\*\* with the National Aeronautics and Space Administration.

#### REFERENCES

- [1] J. Ruze. Antenna tolerance theory — a review. *Proceedings of the IEEE*, 54(4):633–640, April 1966.
- [2] G. Greschik, A. Palisoc, G. Veal, C. Cassapakis, and M. M. Mikulas. Approximating paraboloids with axisymmetric pressurized membranes. In *The 39th AIAA/ASME/ASCE/AHS/ASC Structures, Structural Dynamics, and Materials Conference and AIAA/ASME Adaptive Structures Forum*, volume 4, pages 2772–2782, Long Beach, CA, April 20–23 1998. AIAA-98-2102-CP.
- [3] John M. Hedgepeth. Influence of fabrication tolerances on the surface accuracy of large antenna structures. *AIAA Journal*, 20(5):680–686, May 1982. AIAA 82-4116.
- [4] G. C. Hart and J. D. Collins. The treatment of randomness in finite element modeling. *Transactions of the SAE*, 18(Part 4):2408–2416, 1970. Transactions of the Society of Automotive Engineers.
- [5] G. Greschik, M. M. Mikulas, and R. E. Freeland. The nodal concept of deployment and the scale model testing of its application to a membrane antenna. In *The 40th AIAA/ASME/ASCE/AHS/ASC Structures, Structural Dynamics, and Materials Conference and AIAA/ASME*

*Adaptive Structures Forum*, volume 4, pages 2546–2554, St. Louis, MO, April 12–15 1999. AIAA-99-1523-CP.

- [6] G. Greschik, M. M. Mikulas, and R. E. Freeland. Scale model testing of nonlinear phenomena with emphasis on thin film deployable structures. In S. Pellegrino and S. D. Guest, editors, *IUTAM-IASS Symposium on Deployable Structures: Theory and Applications. Proceedings of the IUTAM Symposium held in Cambridge, UK, September 6–9, 1998*, volume 80 of *Solid Mechanics and its Applications*, pages 127–136, Boston, MA, 2000. Kluwer Academic Publishers.
- [7] W. H. Greene. Effects of random member length errors on the accuracy and internal loads of truss antennas. *Journal of Spacecraft*, 22(5):554–559, September–October 1985. AIAA 82-4116.

|  |  |
|--|--|
| Description  | Scaled quantity $x_s$ as<br>function of unscaled $x$                   |
| <b>The definition of scaling:</b>                            |  |
| global dimensions and lengths                                | $d_s = \lambda_d^{-1} d$   |
| strut length errors  | $e_s = \lambda_e^{-1} e$   |
| member cross section stiffness                               | [immaterial]   |
| <b>Structural responses:</b>                                 |  |
| strain   | $\varepsilon_s = \lambda_d \lambda_e^{-1} \varepsilon$                 |
| stress   | [underdetermined]  |
| all angles of rotation                                       | $\alpha_s = \lambda_d \lambda_e^{-1} \alpha$                           |
| truss beam curvature   | $\kappa_s = \lambda_d^2 \lambda_e^{-1} \kappa$                         |
| displacements  | $u_s = \lambda_e^{-1} u$   |
| antenna <i>rms</i> surface error                             | $\varepsilon_{\text{rms},s} = \lambda_e^{-1} \varepsilon_{\text{rms}}$ |
| all local antenna surface errors<br>as defined for this work | $\epsilon_s = \lambda_e^{-1} \epsilon$                                 |

Table 1: Scaling the global truss geometry and the member length errors.

| normalized<br>error |  | data<br>population | probabilistic<br>distribution | mean | standard<br>deviation |
|---------------------|--|--------------------|-------------------------------|------|-----------------------|
| bay sag             | $s_{\text{bay}} / \Delta l_{\text{max}}$ | 3,465,000          | Gaussian                      | 0.0  | .7669                 |
| bay twist           | $w_{\text{bay}} / \Delta l_{\text{max}}$ | 3,465,000          | Gaussian                      | 0.0  | 1.201                 |
| panel twist         | $w_{\text{pan}} / \Delta l_{\text{max}}$ | 3,500,000          | Gaussian                      | 0.0  | 1.827                 |

Table 2: The statistical characterization of normalized local errors.

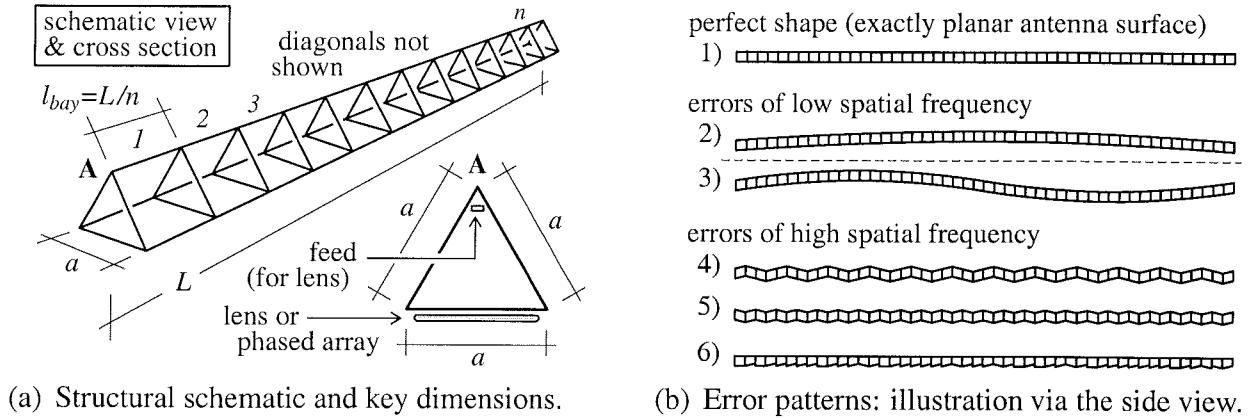


Fig. 1: Schematics of the structure and of some error types.

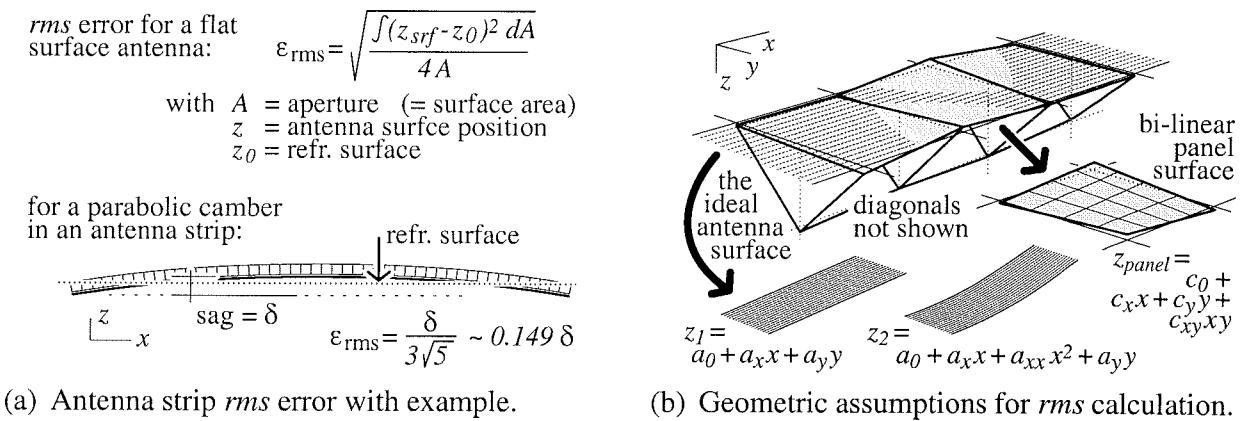


Fig. 2: Surface error definition and the underlying assumptions.

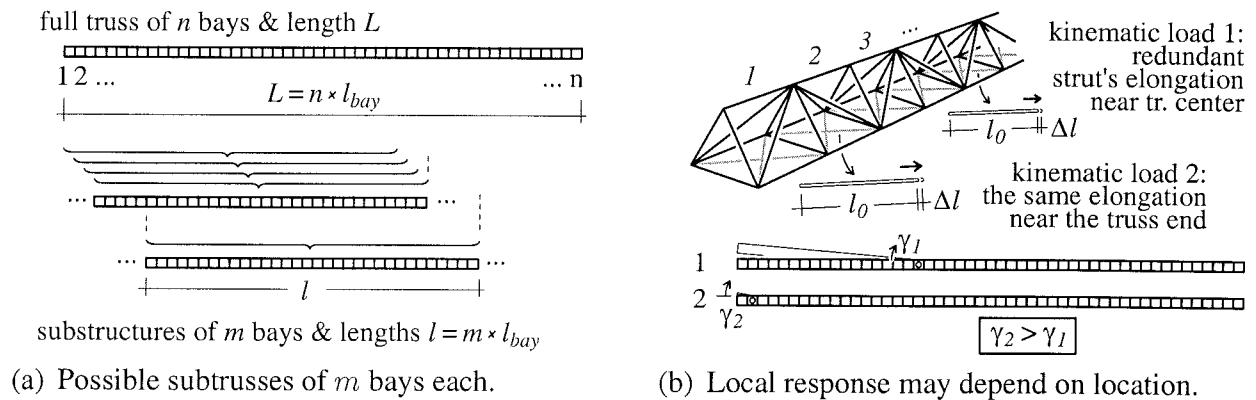
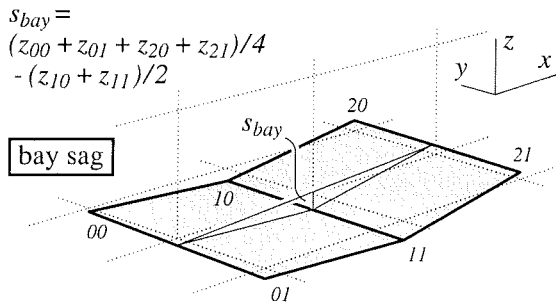
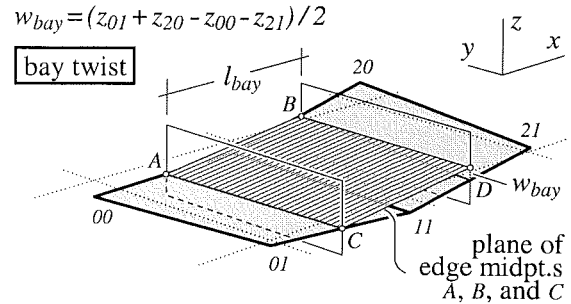


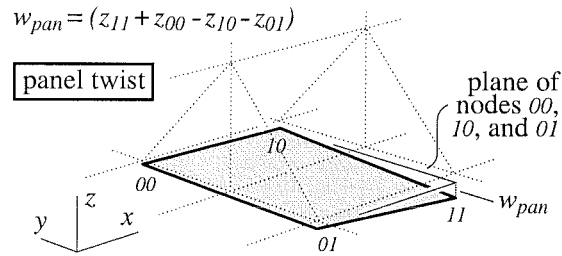
Fig. 3: Subtrusses.



(a) Bay sag  $s_{bay}$ : longitudinal difference between panel orientations.

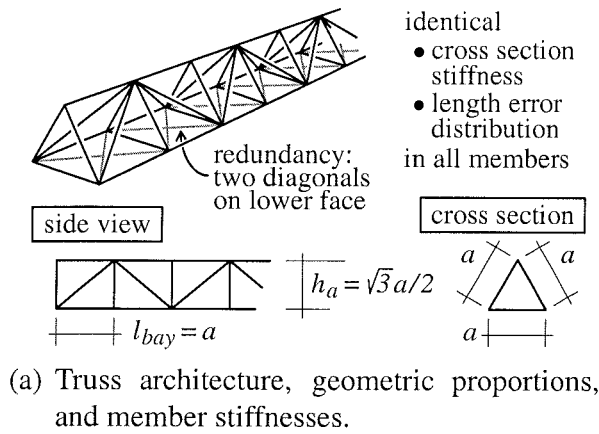


(b) Bay twist  $w_{bay}$ : lateral difference between panel orientations.

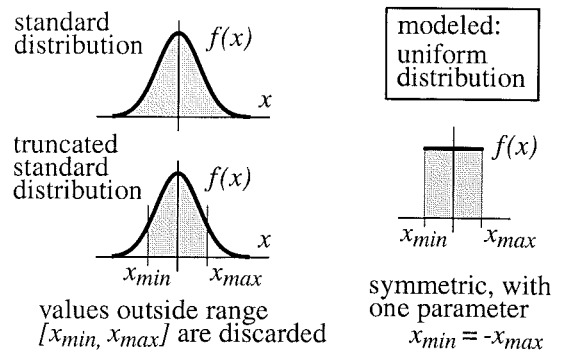


(c) Panel twist: panel out-of-flatness  $w_{pan}$ .

Fig. 4: Local errors, not normalized.



(a) Truss architecture, geometric proportions, and member stiffnesses.



(b) Probability density functions for absolute member length errors.

Fig. 5: Modeling assumptions.

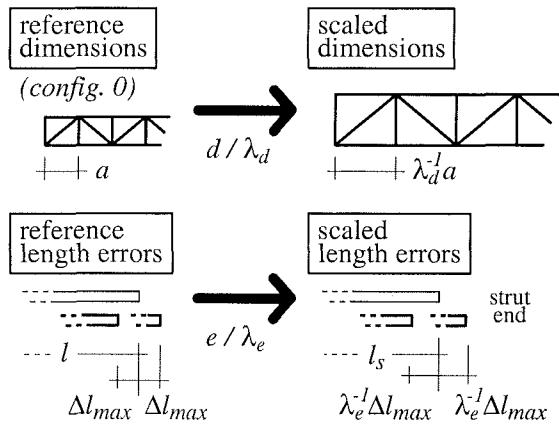


Fig. 6: The scaling of dimensions  $d$  and length errors  $e$  with  $\lambda_d$  and  $\lambda_e$ .

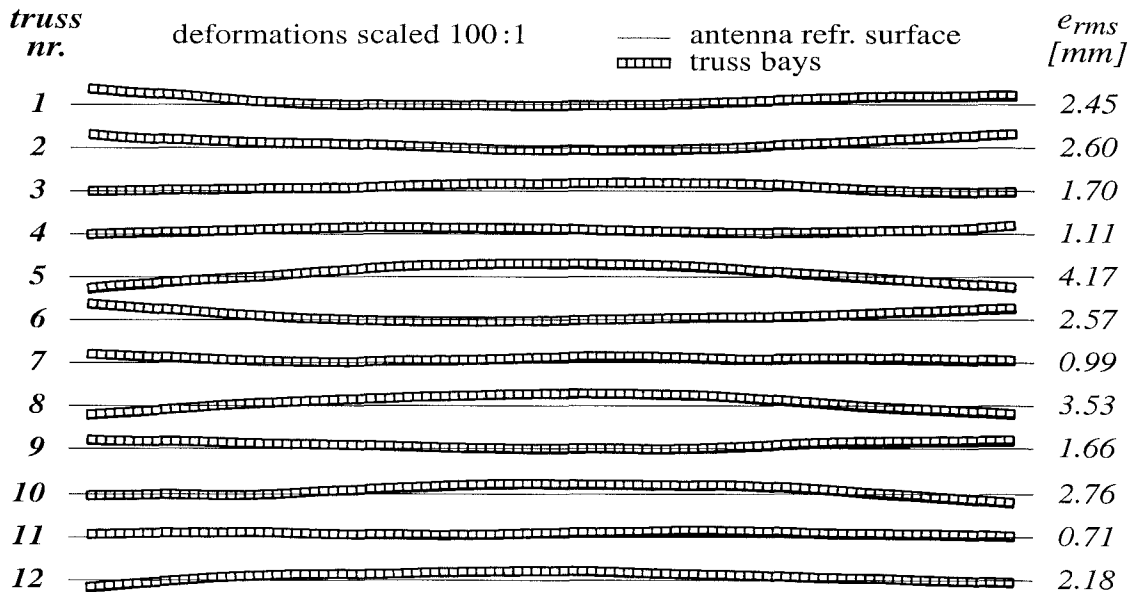


Fig. 7: Some of 35,000 trusses of  $n=100$  bays and batten-, longeron-, and bay lengths of  $1\text{ m}$  with random strut length errors  $\Delta l \in [-0.1, 0.1]\text{ mm}$ . Side view with no diagonals shown.

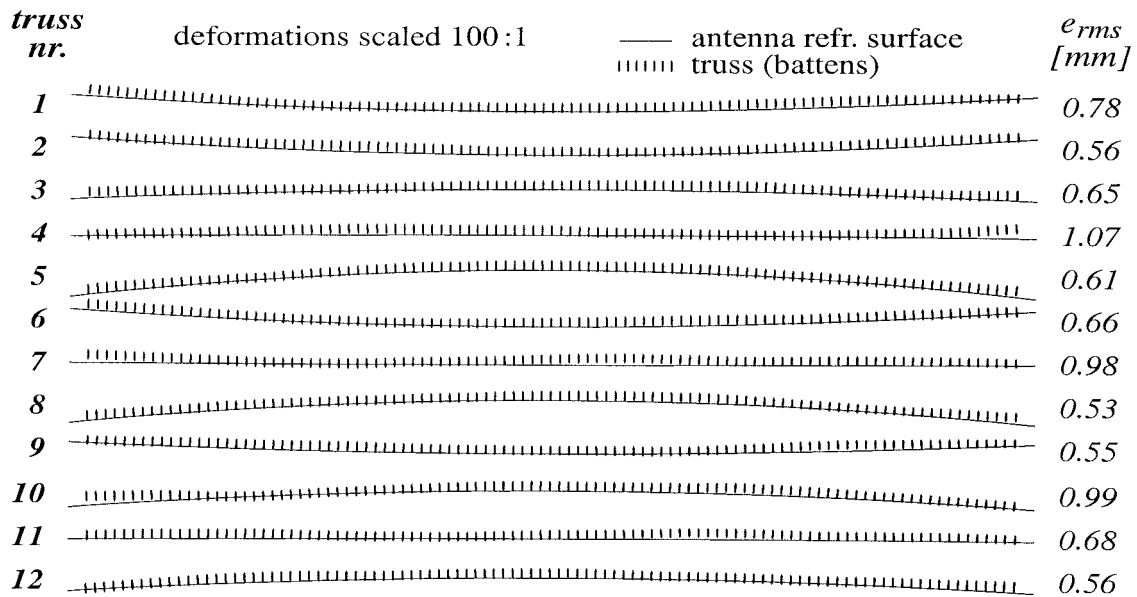


Fig. 8: Parabolic reference surfaces for the trusses in Fig. 7 to simulate quadratic error correction. Side view with longerons and diagonals not shown to avoid graphic congestion.

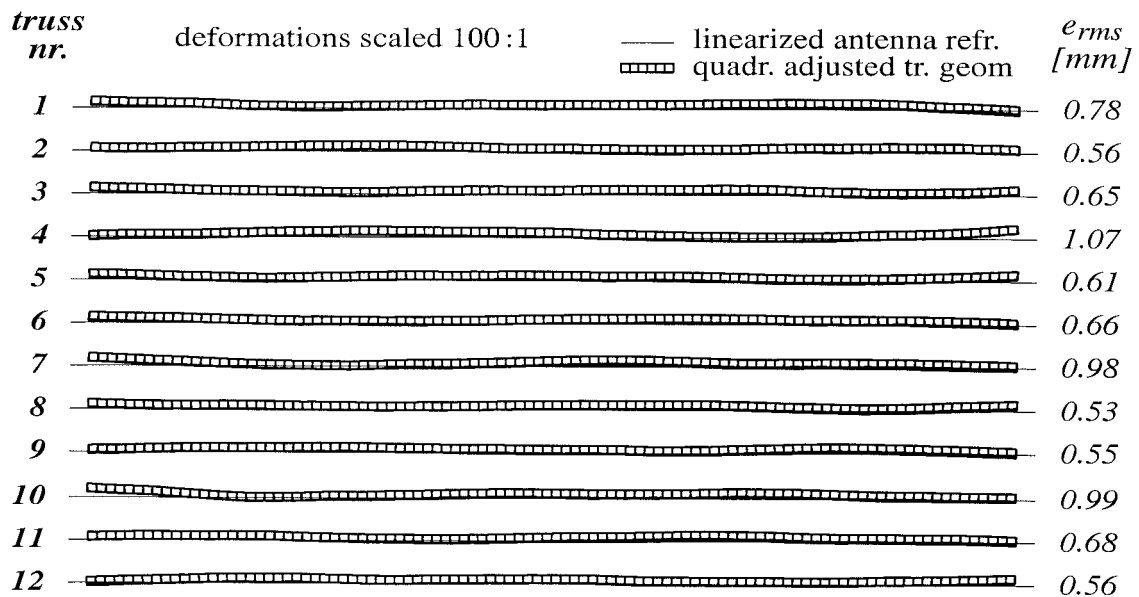
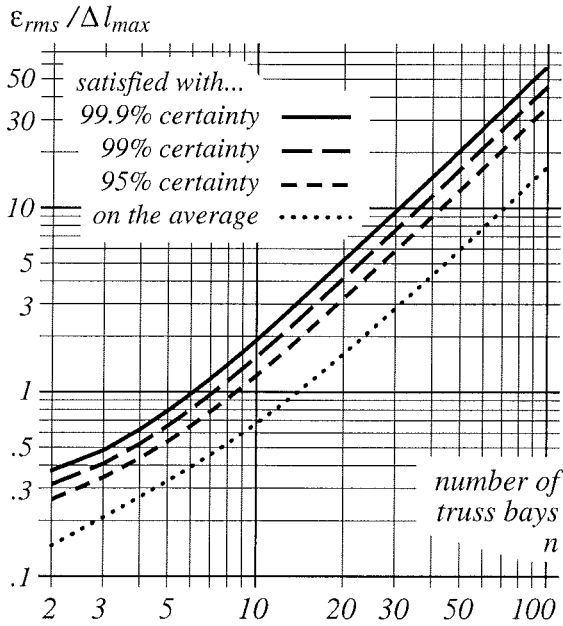
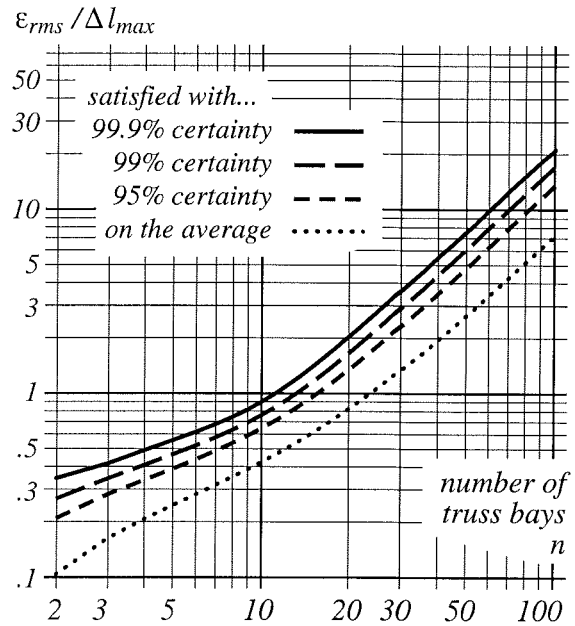


Fig. 9: Offsets from the reference — geometric illustration of the error correction in Fig. 8 via distorting (in the  $z$  direction) the truss and reference geometries to linearize the latter.



(a) Planar reference surface: no error correction.



(b) Quadratic error correction: parabolic reference surface.

Fig. 10: The likelihood of achieving certain threshold surface errors based on a Monte Carlo analysis of 35,000 standard trusses of 100 bays.

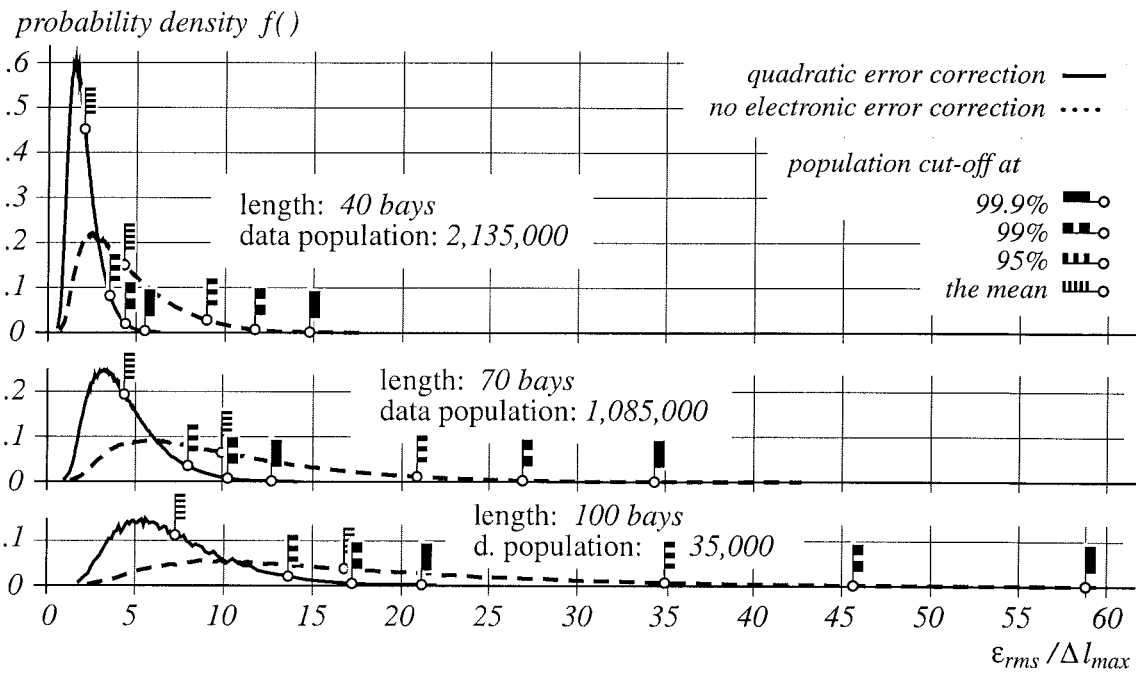


Fig. 11: Probability density functions for some normalized *rms* surface errors.

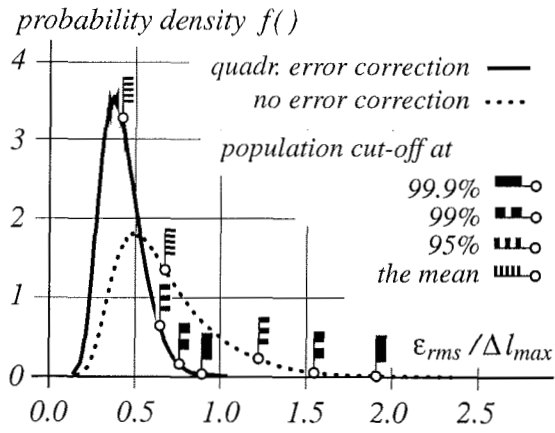


Fig. 12: Probability density of normalized *rms* errors — 10 bays, data pool of 3,185,000.

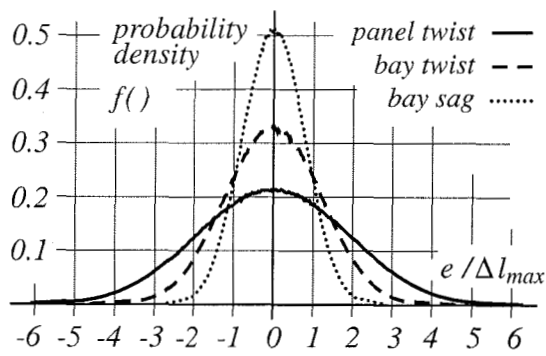
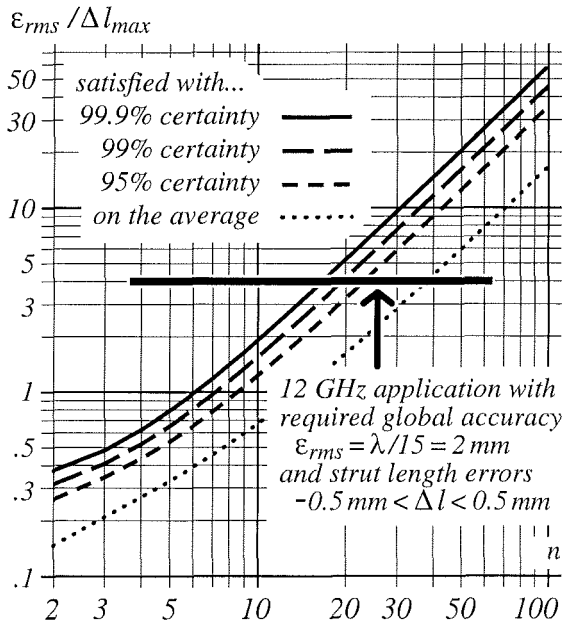
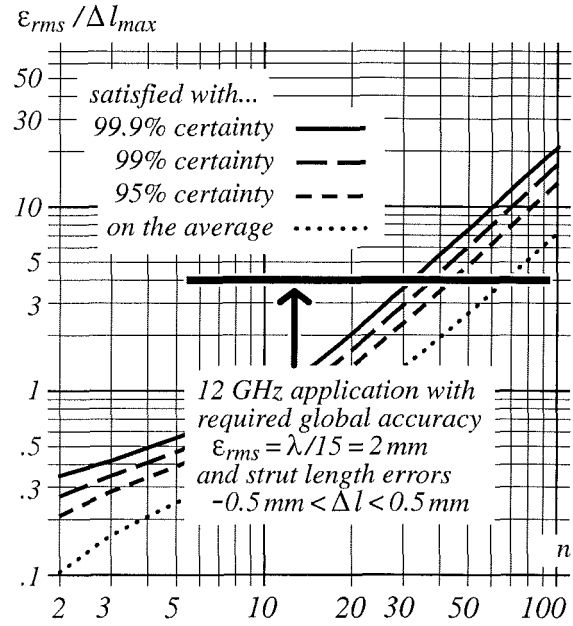


Fig. 13: Probability density functions for local errors, data pool of 3,465,000.

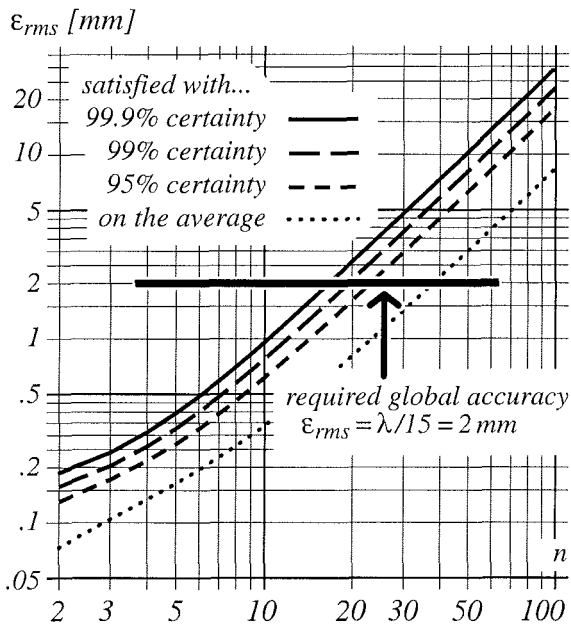


(a) No error correction.

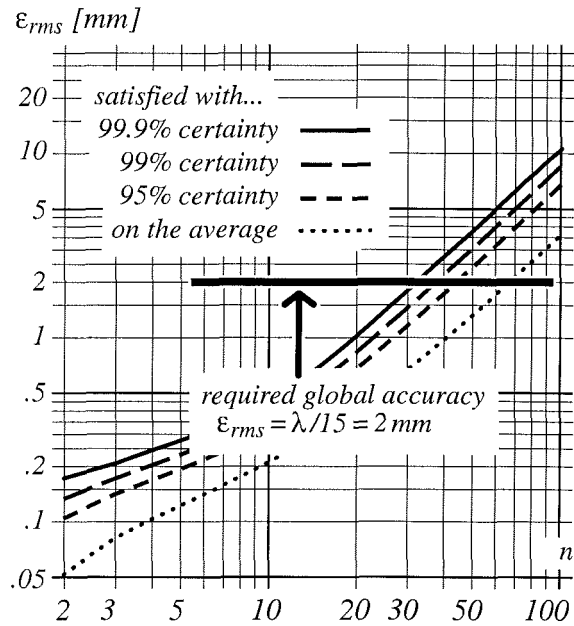


(b) Parabolic error correction.

Fig. 14: Graphical representation of the accuracy requirement for a 12 GHz example application.



(a) No error correction.



(b) Parabolic error correction.

Fig. 15: The accuracy requirement as in Fig. 14 without normalizing the rms error  $\epsilon_{rms}$ .